



Cite as

Nano-Micro Lett.

(2022) 14:30

Received: 24 September 2021

Accepted: 24 November 2021

© The Author(s) 2021

Ultra-Stable and Durable Piezoelectric Nanogenerator with All-Weather Service Capability Based on N Doped 4H-SiC Nanohole Arrays

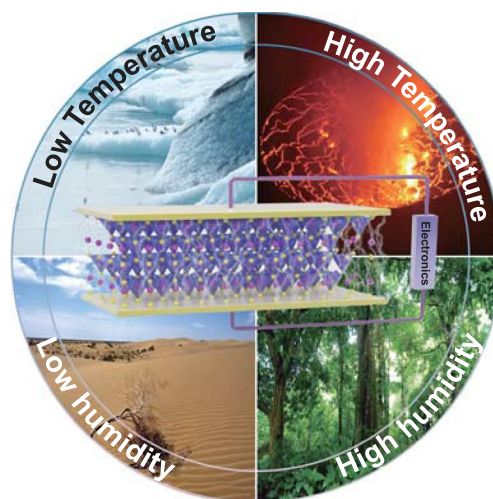
Linlin Zhou¹, Laipan Zhu², Tao Yang¹ ✉, Xinmei Hou¹ ✉, Zhengtao Du³, Sheng Cao³, Hailong Wang⁴, Kuo-Chih Chou¹, Zhong Lin Wang²

HIGHLIGHTS

- An ultra-stable all-weather service piezoelectric nanogenerator (PENG) with a wide operating temperature range (-80~80 °C) and a wide operating relative humidity range (0~100%) is proposed.
- The PENG based on N doped 4H-SiC exhibits long-term service stability up to 50 days.
- The short circuit current density of PENG based on N doped 4H-SiC is enhanced significantly.

ABSTRACT Ultra-stable piezoelectric nanogenerator (PENG) driven by environmental actuation sources with all-weather service capability is highly desirable. Here, the PENG based on N doped 4H-SiC nanohole arrays (NHAs) is proposed to harvest ambient energy under low/high temperature and relative humidity (RH) conditions. Finite element method simulation of N doped 4H-SiC NHAs in compression mode is developed to evaluate the relationship between nanohole diameter and piezoelectric performance. The density of short circuit current of the assembled PENG reaches 313 nA cm^{-2} , which is 1.57 times the output of PENG based on N doped 4H-SiC nanowire arrays. The enhancement can be attributed to the existence of nanohole sidewalls in NHAs. All-weather service capability of the PENG is verified after being treated at -80/80 °C and 0%/100% RH for 50 days. The PENG is promising to be widely used in practice worldwide to harvest biomechanical energy and mechanical energy.

KEYWORDS Piezoelectric nanogenerators; N doped 4H-SiC nanohole arrays; Environmental actuation sources; All-weather service capability; Enhanced short circuit current density



✉ Tao Yang, yangtaoustb@ustb.edu.cn; Xinmei Hou, houxinmeiustb@ustb.edu.cn

¹ Beijing Advanced Innovation Center for Materials Genome Engineering, Collaborative Innovation Center of Steel Technology, University of Science and Technology Beijing, Beijing 100083, People's Republic of China² Beijing Institute of Nanoenergy and Nanosystems, Chinese Academy of Sciences, Beijing 100083, People's Republic of China³ MOE Key Laboratory of New Processing Technology for Non-Ferrous Metals and Materials, Guangxi Key Laboratory of Processing for Non-Ferrous Metals and Featured Materials, Guangxi University, Nanning 530004, People's Republic of China⁴ School of Materials Science Engineering, Zhengzhou University, Zhengzhou 450001, People's Republic of China

1 Introduction

Environmental actuation sources, one of the most widely distributed energy sources in nature, are being explored and developed. Nowadays, nanogenerators (NGs) have been considered favorable candidates for ambient sources harvesting [1–5]. Among them, piezoelectric nanogenerator (PENG) has a tighter connection structure, smaller size and longer service life, making it more suitable for practical applications. Due to the complexity of the Earth's environment, such as from $-70\text{ }^{\circ}\text{C}$ in polar region to $60\text{ }^{\circ}\text{C}$ in Africa, from 0% relative humidity (RH) in desert to 100% RH in rainforest, the PENG with all-weather service capability is in urgent need of development. So, the standards required for piezoelectric materials used to assemble all-weather service PENG, such as chemical and thermal stability, environmental friendliness and durability, have become the main obstacles restricting their wide application [6]. The piezoelectric polymer, for example, PVDF, P(VDF-TrFE) and PVDF-HFP, can't be applied in extreme temperature environments due to thermal instability [7–10]. As for piezoelectric ceramics, i.e., $\text{Pb}(\text{Zr}, \text{Ti})\text{O}_3$ (PZT), $\text{Pb}(\text{Mg}_{1/3}\text{Nb}_{2/3})\text{O}_3$ - PbTiO_3 (PMN-PT), CsPbBr_3 , with high piezoelectric coefficients usually contain lead (Pb), which is harmful to the environment [11–14]. While the lead-free piezoelectric ceramics, i.e., BaTiO_3 , NaNbO_3 usually have complex preparation processes and harsh synthesis conditions, which makes them not suitable for promotion in practical applications [15–18]. In particular, the high brittleness of ceramics makes them easily damaged, limiting their service life severely. In addition to the classic piezoelectric materials, multiple piezoelectric semiconductors such as ZnO [19, 20], GaN [21, 22], MoS_2 [23], and MoSe_2 [24], have been widely investigated to assemble PENG. Among them, the chemical instability of ZnO to acids and bases prevents it from harvesting ambient sources. The preparation process of highly oriented GaN nanoarrays is cumbersome. And the fabrication of uniform monolayer MoS_2 and MoSe_2 is pretty complex to control bonding and crystal, making it impractical for global promotion [25].

SiC, one of the most important third-generation semiconductors with extraordinary chemical and thermal stability, outstanding mechanical properties and good thermal shock resistance, is recognized as one of the potential materials for constructing devices with excellent stability and durability to

service in harsh conditions including high temperature, high pressure, high irradiation and high power [26–29]. Recently, our group has noted the excellent piezoelectric properties of 4H-SiC due to the separation of positive and negative charge centers along c-axis and proposed a PENG based on N doped 4H-SiC nanowire arrays (NWAs) [30, 31]. The stable output under high temperature and high concentration of acid/alkali solutions environments verifies the stability of the PENG based on 4H-SiC. However, in order to obtain the PENG with all-weather service capability, the output performance of the PENG based on 4H-SiC needs to be further improved, the stability (including different temperature and RH) and durability of the PENG need to be further explored.

Herein, an ultra-stable and durable PENG with all-weather service capability and improved output ability was fabricated by N doped 4H-SiC NHAs. The influence of nanohole diameter on structural stability and output ability of the NHAs was studied by finite element method (FEM). Especially, all-weather service capability of the PENG, including high/low temperature and RH, was investigated systematically. The results of practical applications show that N doped 4H-SiC NHAs is one of the most favorable candidates for PENG worked in harsh conditions.

2 Experimental Section

2.1 Materials

The N doped single-crystalline 4H-SiC wafer was obtained from TankeBlue Semiconductor Co. Ltd.. Ethanol ($\text{C}_2\text{H}_5\text{OH}$, 99%) and hydrogen peroxide (H_2O_2 , 30%) were purchased from Sinopharm Chemical Reagent. Hydrofluoric acid (HF, 40%) was from Aladdin in Beijing of China.

2.2 Materials Preparation and Fabrication of PENG

The N doped 4H-SiC NHAs were prepared by anodic oxidation. The etching solution is composed of HF, $\text{C}_2\text{H}_5\text{OH}$ and H_2O_2 with a volume ratio of 6:6:1. The voltage of 21 V with a cycle time (T) of 8 ms and a pause time (T_{off}) of 4 ms was applied for 10 min to form NHAs. The freestanding NHAs film was exfoliated under the function of the direct voltage of 21 V for 60 s and utilized to assemble a well-sealed PENG. PDMS was spin-coated on one side of NHAs and

cured at 80 °C for 20 min and a piece of Al foil was attached to PDMS tightly. The obtained N doped 4H-SiC/PDMS/Al was fixed on another piece of Al foil by silver paste. The sandwich-structure device was fixed on a PET plate and encapsulated with PDMS.

2.3 Characterization and Measurement

The morphology and structure of the NHAs were investigated by field emission scanning electron microscope (FESEM; JSM-6701F, JEOL) and transmission electron microscopy (TEM; JEM-2100, JEOL). The crystal structure of samples was studied by X-ray diffraction (XRD; Smart-Lab/Ultima IV, Rigaku). X-ray photoelectron spectroscopy (XPS; ESCALAB 250Xi, Thermo Fisher Scientific) was used to measure their surface species. Displacement-voltage butterfly loop of NWAs was recorded by the piezoresponse force microscopy (PFM; Dimension Icon, Bruker).

2.4 Simulation Settings

The bottom of the NHAs is treated as grounding and fixing constraints. The top of NHAs with floating potential was rigid and the normal displacement of the side walls was set to zero [32]. And the pressure of 1 MPa was applied on the top surface of NHAs along the *c*-axis.

3 Results and Discussion

The N doped 4H-SiC NHAs were prepared by anodic oxidation of single-crystalline N doped 4H-SiC wafer [33, 34]. The representative fabrication procedure of PENG based on

the exfoliated N doped 4H-SiC NHAs is schematically illustrated in Fig. 1 a-e. The SEM image of the N doped 4H-SiC NHAs in the inset of Fig. 1a reveals the actual nanohole distribution in the arrays. The cross-sectional SEM image reveals the interlayer structure of the PENG (Fig. 1f). And the excellent flexibility of the well-sealed PENG is disclosed in the inset of Fig. 1f.

3.1 Characterization of NHAs

At the beginning of anodic oxidation, extremely small holes appear. HF etching solution tends to enter the bottom of these holes under the electric field perpendicular to the surface of the N doped 4H-SiC sheet. The holes expand gradually and CO₂ gas generated by the oxidation of SiC accumulates on sidewalls, hindering the lateral etching reaction. Yet the longitudinal etching process proceeds normally, forming neatly arranged NHAs perpendicular to the SiC substrates. The larger pore is generated by the corrosion and penetration of the sidewalls between small holes [34]. SEM images show that the N doped 4H-SiC NHAs exhibits a dense nanohole structure with diameters ranging from 14.5 nm to more than 200 nm (Fig. S1a, b). The average diameter of nanohole in arrays is 73.67 nm and most of the apertures are less than 100 nm (Fig. S1c) [35]. The XRD patterns of the NHAs powder confirm that it can be indexed to 4H-SiC (JCPDS Card No. 73–1664) (Fig. S2a). There is only one sharp peak of (004) in the XRD spectrum of N doped 4H-SiC NHAs, disclosing their single-crystalline nature and high crystallinity. Further, the detailed morphology of the as-prepared sample was disclosed by TEM (Fig. S2b). The N doped 4H-SiC NHAs exhibits different widths at different locations, which results from the combined effects of the voltage oscillations,

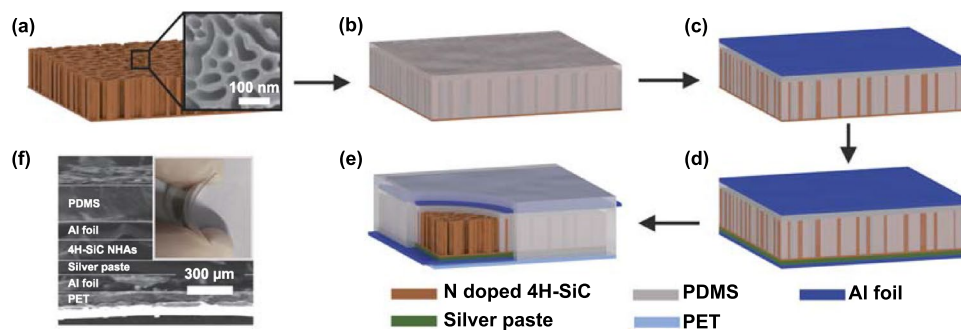


Fig. 1 a–e Schematic diagram of the fabrication process for the PENG. The inset in a is the SEM image of the top-view of N doped 4H-SiC NHAs. f SEM image of the cross-sectional view of the assembled PENG. The inset in the upper right corner is the picture of bending PENG

the periodical etching reaction and the different etching rates of the C and Si faces [34, 36]. The well-arranged crystalline lattice fringes represented in high-resolution TEM (HRTEM) image correspond to the (004) crystal plane of 4H-SiC (Fig. S2c). The select area electron diffraction (SAED) patterns (Fig. S2d) are consistent with XRD results. XPS spectrum of the NHAs reveals that they are composed of C, Si, O, and N (Fig. S3). The O 1 s spectrum indicates the presence of SiO_xC_y and SiO_2 formed during anodizing (Fig. S3d) [26]. And the N dopants incorporated into 4H-SiC lattice are revealed by N 1 s fine XPS spectrum (Fig. S3e).

Further, the displacement-voltage butterfly loops of 4H-SiC and N doped 4H-SiC verify that the N doped 4H-SiC exhibits more significant piezoelectric properties (Fig. S4). Actually, 4H-SiC belongs to hexagonal $P6_3mc$ space-group symmetry with a wurtzite structure. The tetrahedral unit of 4H-SiC is composed of one Si atom and four C atoms coordinated with the Si atom. In this unit, the apical bond length of Si-C is 1.890 Å (parallel to the c-axis) yet the basal one is 1.880 Å. The distortion of the tetrahedron along c-axis leads to the separation of the cation and anion centers of 4H-SiC, forming c-axis-oriented dipole moments. Once an external force is applied along the c-axis, the deformation of the tetrahedral units of 4H-SiC will significantly strengthen the dipole moments and enhance piezoelectricity [31, 37–39]. Furthermore, N doping will enhance the piezoelectricity of 4H-SiC by adjusting crystal structure and inducing dipoles. On one hand, the lattice distortion caused by the introduction of N atoms in 4H-SiC lattice increases the asymmetry of the wurtzite structure [40]. On the other hand, the remaining electrons of N atoms tend to become free electrons. The electron-losing N ion makes the surrounding positively charged center shift, forming a dipole. These dipoles will emerge orientation polarization under the force field, resulting in an enhanced piezoelectric effect [41]. Hence, the N doped 4H-SiC possesses more significant piezoelectricity.

3.2 FEM Simulation of NHAs

To further investigate the piezoelectric effect of the N doped 4H-SiC NHAs, a finite element method (FEM) simulation was performed by the COMSOL Multiphysics software [32, 42, 43]. The geometry schematic of N doped 4H-SiC NHAs with the size of $1\ \mu\text{m} \times 1\ \mu\text{m} \times 200\ \text{nm}$ is presented in Fig. 2a. The aperture of nanoholes in NHAs was set to vary from 40 to 200 nm according to the statistical distribution of nanoholes (Fig. S1c). The electric potential (V) of the N doped 4H-SiC NHAs is uniformly distributed (Fig. 2b) and the peak value of $V(V_{\text{max}})$ reaches $-4.89\ \text{mV}$. To distinguish the contribution of nanoholes with different apertures to performance, five NHAs units with diameters of 20, 40, 80, 100, and 200 nm were established (Fig. S5). The tendency of maximum displacement (D_{max}) and $|V_{\text{max}}|$ of NHAs with increasing diameters are represented in Fig. 2c. When the same pressure is applied, the displacement and electric potential increase nonlinearly with the enlargement of nanohole diameters. Although the larger displacement of NHAs will induce better electrical output performance, the resulting giant structural deformation will greatly limit their service life in practice. Especially, the trend of electric potential and deformation growth slows down as the aperture increases. As for the as-prepared N doped 4H-SiC NHAs, the smaller holes will improve the structural stability and the larger holes can optimize the piezoelectric performance. Therefore, the NHAs with a diameter within the range of 20 to 200 nm approximately are suitable for assembling PENG. As the anodizing time increases, the nanohole size expands and the sidewalls of the holes in NHAs gradually collapse to form NWAs. Hence, the structural stability of the 4H-SiC NWAs is inevitably worse than that of the NHAs, making them inapplicable in practice.

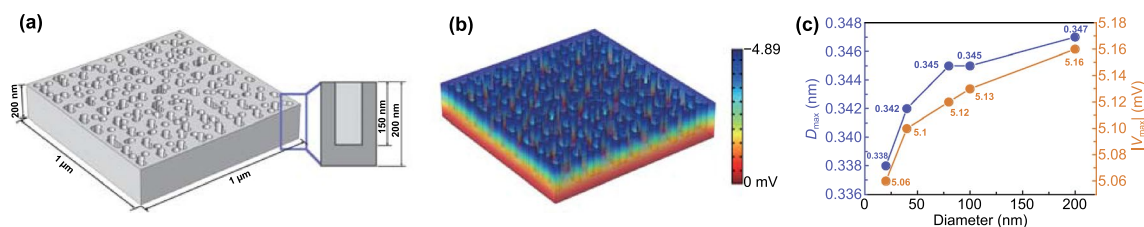


Fig. 2 **a** Geometry Schematics of the N doped 4H-SiC NHAs. **b** Distribution of the V in NHAs at a pressure of 1 MPa. **c** The tendency of D_{max} and $|V_{\text{max}}|$ with the increase of nanohole diameters

3.3 Performance Test of PENG

When a force of 0.6 N is applied, the density of I_{sc} and open circuit voltage (V_{oc}) of the assembled PENG are 108 nA cm^{-2} and 1.35 V, respectively (Fig. 3a, b). A blank PENG without N doped 4H-SiC NHAs was constructed to verify the effective piezoelectric output of NHAs. Compared with the PENG based on N doped 4H-SiC NHAs, the blank one shows a negligible signal generated by the noise in surrounding environments (Fig. S6). Hence, it can be concluded that the electrical signals originate from the piezoelectric effect of N doped 4H-SiC NHAs.

The performance of PENG based on N doped 4H-SiC NHAs under actual working conditions was evaluated by changing the force and frequency of the external stimulus. The density of I_{sc} rises from 108 to 313 nA cm^{-2} with external force increasing from 0.6 to 4.9 N. And then, the current remains constant as the force increases (Fig. 3c). When the force is less than 4.9 N, the deformation of the NHAs possibly increases with the increase of the force, resulting in an enhanced polarization and larger output. Once the force reaches 4.9 N or above, it might be difficult for NHAs to produce greater deformation and stronger polarization. Thus the forward output will no longer improve with the increase of force but stabilize at a

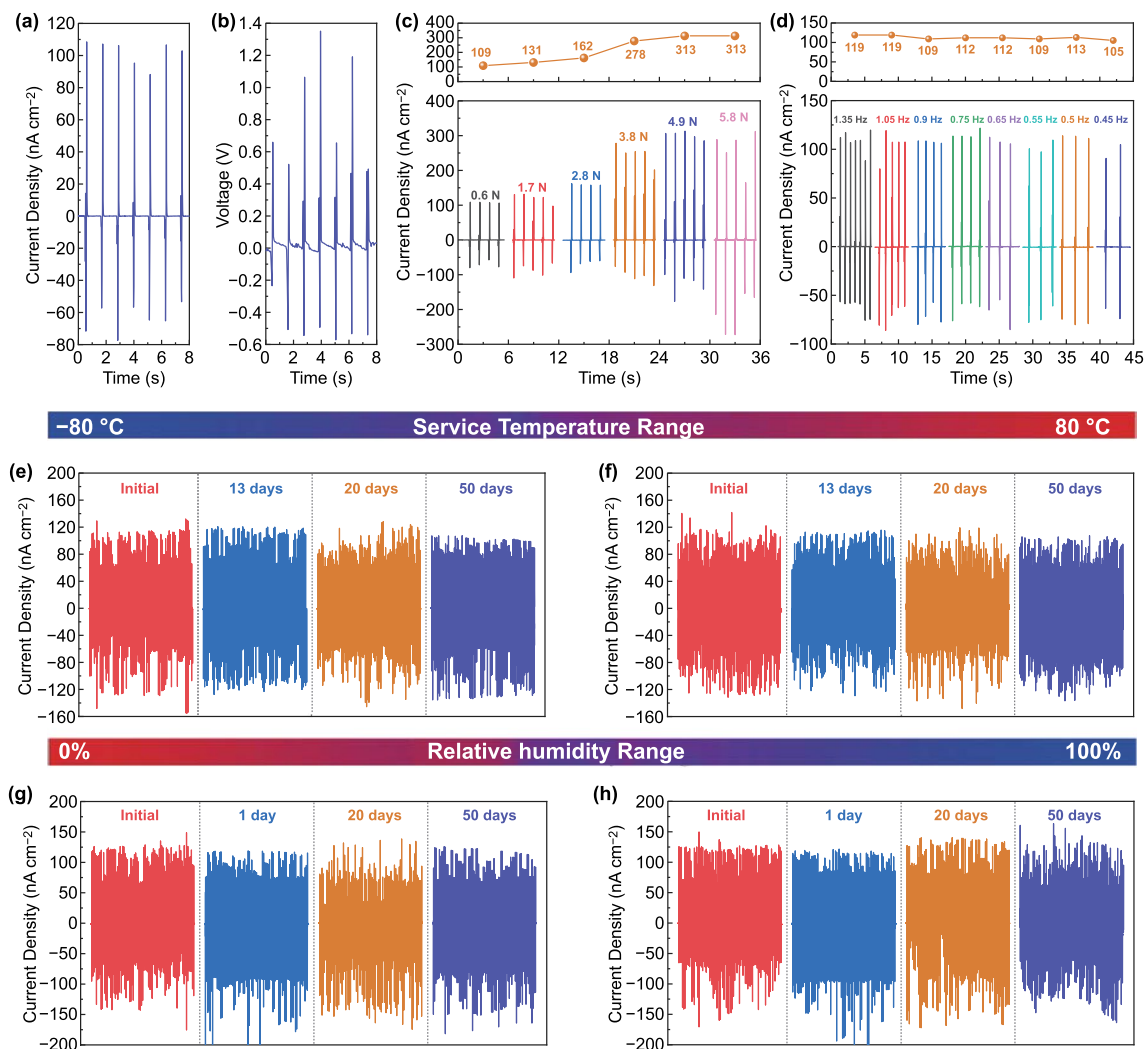


Fig. 3 **a** Density of I_{sc} and **b** V_{oc} of the PENG. The density of I_{sc} and the output trend of PENG based on N doped 4H-SiC NHAs under different external stimulus; **c** various forces and **d** various frequencies. The long-term stability of as-constructed PENG within up to 50 days under different temperatures and RHs: **e** -80, **f** 80 °C, **g** 0% RH, and **h** 100% RH

fixed value [34]. It should be noted that subsequent tests are all carried out under the external force of 0.6 N. The PENG shows excellent stability under frequency interference in the range of 0.45 to 1.35 Hz (Fig. 3d). As frequency increases, the density of I_{sc} of the PENG fluctuates slightly within the range of 105 to 119 nA cm⁻². The changing rate of dipole moments in NHAs is not affected by frequency fluctuations of external stimuli. So that both the escaped charges and the accumulated charges on surface remain unchanged, resulting in a stable output [44]. The insensitivity to frequency allows the as-prepared PENG to be applied in situations with multiple interference factors, such as heavy rains and typhoons.

Further, the PENG is verified to be capable of working normally after being frozen at -80 °C (Fig. 3e) and heated at 80 °C for 50 days (Fig. 3f). There is no significant drop during the imparting and releasing processes throughout the long-term stability test, indicating the ultra-stability and durability of the PENG. Hence, the PENG can be utilized as an energy harvester to collect and transfer irregular environmental actuation sources in our living environment for a long period. In addition, The PENG also shows a stable output within the RH range of 0 to 100% for 50 days (Fig. 3g, h). As a result, the ultra-stable and durable PENG with all-weather service capability based on N doped 4H-SiC NHAs is proven to be applicable worldwide.

The load capacity of PENG was monitored by measuring V_{oc} across the resistor connected to the PENG. The peak value of V_{oc} increases nonlinearly from 0.014 to 0.574 V with the external load ranging from 1 to 100 M Ω (Fig. S7a, b). And the power density of PENG rises with the resistances increase from 1 to 30 M Ω and then decreases once the external load exceeds 30 M Ω . The NHAs-based PENG exhibits a maximum power density value of 26.52 nW cm⁻² when the resistance of 30 M Ω is connected. Notably, the electrical energy converted from mechanical energy by PENG can be stored in capacitors through a bridge rectifier. The pulsed electrical signals are converted into forward voltage by a rectifier circuit (Fig. S7c). A 100 μ F capacitor is charged to 0.033 V by the PENG within 800 s (Fig. S7d), proving the feasibility of the PENG to be applied in practical applications.

3.4 Environmental Energy Harvesting

Here, the PENG was used to harvest biomechanical energy, i.e. finger tapping, foot striking and mechanical energy, i.e.,

cantilever beam, simulated automobile exhaust emission. When the PENG is subjected to finger tapping and foot striking, the density of I_{sc} reaches 45 and 318 nA cm⁻², respectively (Fig. S8a, b). The mechanical energy generated from the vibration of the simulated cantilever beam can be converted to electrical energy by the PENG (55 nA cm⁻², Fig. S8c). Besides, the automobile exhaust emission process was simulated by air blower and the PENG was used to harvest the wind and vibration energy simultaneously (-116 nA cm⁻², Fig. S8d). The thermal stability of N doped 4H-SiC breaks through the limitation of high temperature conditions, making the N doped 4H-SiC NHAs-based PENG can be applied to harvest multiple energy sources during the automobile exhaust emission process.

The key performance of N doped 4H-SiC NHAs-based PENG is compared with PENGs constructed by various material systems, i.e., lead-based perovskite, lead-free perovskite, piezoelectric polymer and piezoelectric semiconductor (Table 1). Notably, the density of I_{sc} of the PENG based on N doped 4H-SiC NHAs is basically the same as that of some PENGs assembled by classic piezoelectric materials, such as CsPbBr₃/P(VDF-TrFE) [45], BiFeO₃ [46], ZnO [20] and GaN [21, 22]. Most importantly, PENG based on N doped 4H-SiC NHAs possesses a wider service temperature range (-80 ~ 80 °C), wider operating RH range (0 ~ 100%) and longer service life (50 days), indicating the all-weather service capability. In addition, the N doped 4H-SiC has been verified to be capable of working at 200 °C in our previous work [30]. The wide service temperature and RH range of the N doped 4H-SiC is of great significance to the practical application of PENG.

The ultra-stability and enhanced performance of the PENG based on N doped 4H-SiC NHAs can be attributed to the following points. Firstly, the intrinsic properties of N doped 4H-SiC. The wide band gap, stable physical/chemical properties and intrinsic piezoelectricity of N doped 4H-SiC enable it to adapt to various extreme environments. Secondly, the nanostructure of the as-prepared NHAs. On one hand, the NHAs composed of nanoholes with different diameters exhibit both excellent structural stability and significant electrical output. On the other hand, the NHAs undergo anodic oxidation in a short period and retain the sidewalls. There are more SiC units in NHAs to produce dipoles in crystals when subjected to external stimuli, resulting in an enhanced macroscopic current output. Finally, the

Table 1 The key performance of PENGs based on various materials

Materials	Mode	I_{sc}	Service temperature (°C)	Relative humidity	Stable service time	Refs
Lead-based perovskite	PZT	Bending	$10.9 \mu\text{A cm}^{-2}$	RT	Air	50,000 cycles [47]
	PZT	Pressing	$17.5 \mu\text{A}$	RT	Air	– [48]
	PMN-PT	Pressing	$290 \mu\text{A cm}^{-2}$	RT	Air	– [12]
	CsPbBr ₃ /P(VDF-TrFE)	Pressing	$0.17 \mu\text{A}$	RT	Air	– [45]
Lead-free perovskite	BaTiO ₃	Pressing	$2.9 \mu\text{A}$	RT	Air	14 days [49]
	BiFeO ₃	Pressing	$\sim 250 \text{ nA}$	RT	Air	1000 cycles [46]
	NaNbO ₃	Pressing	16 nA cm^{-2}	RT	Air	30 h [17]
Piezoelectric polymer	PVDF	Pressing	$> 0.7 \mu\text{A}$	RT	Air	– [7]
	P(VDF-TrFE)/GeSe	Pressing	$1.14 \mu\text{A}$	RT	Air	– [8]
	P(VDF-HFP)	Pressing	$0.9 \mu\text{A cm}^{-2}$	RT	Air	– [9]
Piezoelectric semiconductor	ZnO	Pressing	$7.2 \mu\text{A cm}^{-2}$	RT	Air	– [19]
	ZnO	Pressing	36 nA	RT	Air	– [20]
	ZnO/AlN	Pressing	$1.10 \mu\text{A}$	RT	Air	– [50]
	GaN	Bending	85.6 nA	RT	Air	20,000 cycles [21]
	GaN	Pressing	150 nA	RT	Air	– [22]
	AlN	Bending	$1.6 \mu\text{A}$	RT	Air	1800 cycles [51]
	MoS ₂	Bending	–	RT	Air	$\sim 175 \text{ s}$ [23]
	MoSe ₂	Bending	–	RT	Air	$> 1500 \text{ s}$ [24]
	N doped 4H-SiC NWAs	Pressing	200 nA cm^{-2}	25~200	Air	20,000 cycles [30] Our previous work
	N doped 4H-SiC NHAs	Pressing	313 nA cm^{-2}	–80~80 (200)	0~100%	50 days This work

Materials-types of materials used to assemble PENGs; Mode-the working mode of the PENG, mainly including pressing and bending; I_{sc} -short circuit current of the PENG; Service temperature-the temperature range in which the PENG works normally; Relative humidity-the humidity range in which the PENG works normally; Stable service time-the service life of the PENG in normal operation; Refs-corresponding references

well-sealed structure of the PENG. The as-prepared PENG is completely wrapped to isolate external pollutions and prevent the structure from being damaged.

4 Conclusions

In summary, an ultra-stable PENG based on N doped 4H-SiC NHAs with all-weather service ability is demonstrated. The assembled PENG shows the density of I_{sc} and V_{oc} of 108 nA cm^{-2} and 1.35 V when subjected to an external force of 0.6 N . Once a force of 4.9 N is applied, it produces the density of I_{sc} of 313 nA cm^{-2} , which is 1.57 times the output of that assembled by NWAs (200 nA cm^{-2}). The FEM simulation results reveal that the deformation and the electric potential of the NHAs both

increase with the enlargement of the aperture. And the PENG based on NHAs with diameters ranging from 20 to 200 nm approximately possess excellent structural stability and enhanced short circuit current density. The PENG can effectively resist the interference caused by frequency varying from 0.45 to 1.35 Hz. And the PENG maintains high output after being treated at $-80/80 \text{ }^\circ\text{C}$ and 0%/100% RH for 50 days. It realizes the conversion from mechanical energy to electricity by harvesting ambient energy generated by finger tapping, foot striking, cantilever beam and simulated automobile exhaust emission. The ultra-stable and durable PENG based on the N doped 4H-SiC NHAs can harvest environmental actuation sources effectively and is of great significance for the development of self-powered systems.

Acknowledgements Linlin Zhou and Laipan Zhu contributed equally to this work. This work was supported by the National Science Fund for Distinguished Young Scholars (No. 52025041), the National Natural Science Foundation of China (No. 51974021, 51902020, 51904021), the Fundamental Research Funds for the Central Universities of NO. FRF-TP-18-045A1 and FRF-TP-19-004B2Z, the National Postdoctoral Program for Innovative Talents (BX20180034). This project is supported by open foundation of Guangxi Key Laboratory of Processing for Non-ferrous Metals and Featured Materials, Guangxi University (Grant No. 2021GXYSOF12).

Funding Open access funding provided by Shanghai Jiao Tong University.

Open Access This article is licensed under a Creative Commons Attribution 4.0 International License, which permits use, sharing, adaptation, distribution and reproduction in any medium or format, as long as you give appropriate credit to the original author(s) and the source, provide a link to the Creative Commons licence, and indicate if changes were made. The images or other third party material in this article are included in the article's Creative Commons licence, unless indicated otherwise in a credit line to the material. If material is not included in the article's Creative Commons licence and your intended use is not permitted by statutory regulation or exceeds the permitted use, you will need to obtain permission directly from the copyright holder. To view a copy of this licence, visit <http://creativecommons.org/licenses/by/4.0/>.

Supplementary Information The online version contains supplementary material available at <https://doi.org/10.1007/s40820-021-00779-0>.

References

1. D. Zhang, D. Wang, Z. Xu, X. Zhang, Y. Yang et al., Diversiform sensors and sensing systems driven by triboelectric and piezoelectric nanogenerators. *Coord. Chem. Rev.* **427**, 213597 (2021). <https://doi.org/10.1016/j.ccr.2020.213597>
2. D. Wang, D. Zhang, Y. Yang, Q. Mi, J. Zhang et al., Multifunctional latex/polytetrafluoroethylene-based triboelectric nanogenerator for self-powered organ-like MXene/metal-organic framework-derived CuO nanohybrid ammonia sensor. *ACS Nano* **15**(2), 2911–2919 (2021). <https://doi.org/10.1021/acsnano.0c09015>
3. D. Wang, D. Zhang, J. Guo, Y. Hu, Y. Yang et al., Multifunctional poly(vinyl alcohol)/Ag nanofibers-based triboelectric nanogenerator for self-powered MXene/tungsten oxide nanohybrid NO₂ gas sensor. *Nano Energy* **89**, 106410 (2021). <https://doi.org/10.1016/j.nanoen.2021.106410>
4. Z. Wang, X. Pan, Y. He, Y. Hu, H. Gu et al., Piezoelectric nanowires in energy harvesting applications. *Adv. Mater. Sci. Eng.* **2015**, 1 (2015). <https://doi.org/10.1155/2015/165631>
5. S. Siddiqui, D.I. Kim, L.T. Duy, M.T. Nguyen, S. Muhammad et al., High-performance flexible lead-free nanocomposite piezoelectric nanogenerator for biomechanical energy harvesting and storage. *Nano Energy* **15**, 177–185 (2015). <https://doi.org/10.1016/j.nanoen.2015.04.030>
6. M.A. Johar, A. Waseem, M.A. Hassan, I.V. Bagal, A. Abdullah et al., Highly durable piezoelectric nanogenerator by heteroepitaxy of GaN nanowires on Cu foil for enhanced output using ambient actuation sources. *Adv. Energy Mater.* **10**(47), 2002608 (2020). <https://doi.org/10.1002/aenm.202002608>
7. V. Khurana, R.R. Kisannagar, S.S. Domala, D. Gupta, In situ polarized ultrathin PVDF film-based flexible piezoelectric nanogenerators. *ACS Appl. Electron. Mater.* **2**(10), 3409–3417 (2020). <https://doi.org/10.1021/acsaem.0c00667>
8. W. Zhai, Q. Lai, L. Chen, L. Zhu, Z.L. Wang, Flexible piezoelectric nanogenerators based on P(VDF-TrFE)/GeSe nanocomposite films. *ACS Appl. Electron. Mater.* **2**(8), 2369–2374 (2020). <https://doi.org/10.1021/acsaem.0c00525>
9. D. Mandal, K. Henkel, D. Schmeisser, Improved performance of a polymer nanogenerator based on silver nanoparticles doped electrospun P(VDF-HFP) nanofibers. *Phys. Chem. Chem. Phys.* **16**(22), 10403–10407 (2014). <https://doi.org/10.1039/c3cp55238a>
10. J.H. Lee, K.Y. Lee, M.K. Gupta, T.Y. Kim, D.Y. Lee et al., Highly stretchable piezoelectric-pyroelectric hybrid nanogenerator. *Adv. Mater.* **26**(5), 765–769 (2014). <https://doi.org/10.1002/adma.201303570>
11. H. Lee, H. Kim, D.Y. Kim, Y. Seo, Pure piezoelectricity generation by a flexible nanogenerator based on lead zirconate titanate nanofibers. *ACS Omega* **4**(2), 2610–2617 (2019). <https://doi.org/10.1021/acsomega.8b03325>
12. L. Gu, J. Liu, N. Cui, Q. Xu, T. Du et al., Enhancing the current density of a piezoelectric nanogenerator using a three-dimensional intercalation electrode. *Nat. Commun.* **11**, 1030 (2020). <https://doi.org/10.1038/s41467-020-14846-4>
13. H. Chen, L. Zhou, Z. Fang, S. Wang, T. Yang et al., Piezoelectric nanogenerator based on in situ growth all-inorganic CsPbBr₃ perovskite nanocrystals in PVDF fibers with long-term stability. *Adv. Funct. Mater.* **31**(19), 2011073 (2021). <https://doi.org/10.1002/adfm.202011073>
14. A.J. Joseph, N. Sinha, S. Goel, A. Hussain, B. Kumar, True-remanent, resistive-leakage and mechanical studies of flux grown 0.64PMN-0.36PT single crystals. *Arab. J. Chem.* **13**(1), 2596–2610 (2020). <https://doi.org/10.1016/j.arabjc.2018.06.012>
15. Y. Wang, X. Zhang, X. Guo, D. Li, B. Cui et al., Hybrid nanogenerator of BaTiO₃ nanowires and CNTs for harvesting energy. *J. Mater. Sci.* **53**, 13081–13089 (2018). <https://doi.org/10.1007/s10853-018-2540-9>
16. Y. Zhao, Q. Liao, G. Zhang, Z. Zhang, Q. Liang et al., High output piezoelectric nanocomposite generators composed of oriented BaTiO₃ NPs@PVDF. *Nano Energy* **11**, 719–727 (2015). <https://doi.org/10.1016/j.nanoen.2014.11.061>
17. J.H. Jung, M. Lee, J.I. Hong, Y. Ding, C.Y. Chen et al., Lead-free NaNbO₃ nanowires for a high output piezoelectric nanogenerator. *ACS Nano* **5**(12), 10041–10046 (2011). <https://doi.org/10.1021/nn2039033>

18. G. Ray, N. Sinha, S. Bhandari, B. Kumar, Excellent piezo-/pyro-/ferroelectric performance of Na_{0.47}K_{0.47}Li_{0.06}NbO₃ lead-free ceramic near polymorphic phase transition. *Scripta Mater.* **99**, 77–80 (2015). <https://doi.org/10.1016/j.scriptamat.2014.11.033>
19. Y. Sun, Y. Zheng, R. Wang, J. Fan, Y. Liu, Direct-current piezoelectric nanogenerator based on two-layer zinc oxide nanorod arrays with equal c-axis orientation for energy harvesting. *Chem. Eng. J.* **426**, 131262 (2021). <https://doi.org/10.1016/j.cej.2021.131262>
20. M. Manikandan, P. Rajagopalan, N. Patra, S. Jayachandran, M. Muralidharan et al., Development of Sn-doped ZnO based ecofriendly piezoelectric nanogenerator for energy harvesting application. *Nanotechnology* **31**, 185401 (2020). <https://doi.org/10.1088/1361-6528/ab6b9e>
21. M.A. Johar, M.A. Hassan, A. Waseem, J.S. Ha, J.K. Lee et al., Stable and high piezoelectric output of GaN nanowire-based lead-free piezoelectric nanogenerator by suppression of internal screening. *Nanomaterials* **8**(6), 437 (2018). <https://doi.org/10.3390/nano8060437>
22. J.H. Kang, D.K. Jeong, S.W. Ryu, Transparent, flexible piezoelectric nanogenerator based on GaN membrane using electrochemical lift-off. *ACS Appl. Mater. Interfaces* **9**(12), 10637–10642 (2017). <https://doi.org/10.1021/acsami.6b15587>
23. D. Zhang, Z. Yang, P. Li, M. Pang, Q. Xue, Flexible self-powered high-performance ammonia sensor based on Au-decorated MoSe₂ nanoflowers driven by single layer MoS₂-flake piezoelectric nanogenerator. *Nano Energy* **65**, 103974 (2019). <https://doi.org/10.1016/j.nanoen.2019.103974>
24. D. Wang, D. Zhang, P. Li, Z. Yang, Q. Mi et al., Electrospinning of flexible poly(vinyl alcohol)/MXene nanofiber-based humidity sensor self-powered by monolayer molybdenum diselenide piezoelectric nanogenerator. *Nano-Micro Lett.* **13**, 57 (2021). <https://doi.org/10.1007/s40820-020-00580-5>
25. B.H. Kang, S.J. Jung, S. Hong, I.S. Lee, S. Hong et al., Improvement of the stability and optoelectronic characteristics of molybdenum disulfide thin-film transistors by applying a nitrocellulose passivation layer. *J. Inf. Display* **21**(2), 123–130 (2020). <https://doi.org/10.1080/15980316.2019.1710585>
26. W. Li, Q. Liu, S. Chen, Z. Fang, X. Liang et al., Single-crystalline integrated 4H-SiC nanochannel array electrode: toward high-performance capacitive energy storage for robust wide-temperature operation. *Mater. Horiz.* **5**(5), 883–889 (2018). <https://doi.org/10.1039/c8mh00474a>
27. T. Yang, S. Chen, X. Li, X. Xu, F. Gao et al., High-performance SiC nanobelt photodetectors with long-term stability against 300 °C up to 180 days. *Adv. Funct. Mater.* **29**(11), 1806250 (2019). <https://doi.org/10.1002/adfm.201806250>
28. W. Liu, J. Chen, T. Yang, K.C. Chou, X. Hou, Enhancing photoluminescence properties of SiC/SiO₂ coaxial nanocables by making oxygen vacancies. *Dalton Trans.* **45**(34), 13503–13508 (2016). <https://doi.org/10.1039/c6dt02049f>
29. H. Dong, Z. Fang, T. Yang, Y. Yu, D. Wang et al., Single crystalline 3C-SiC whiskers used for electrochemical detection of nitrite under neutral condition. *Ionics* **22**, 1493–1500 (2016). <https://doi.org/10.1007/s11581-016-1666-5>
30. L. Zhou, T. Yang, L. Zhu, W. Li, S. Wang et al., Piezoelectric nanogenerators with high performance against harsh conditions based on tunable N doped 4H-SiC nanowire arrays. *Nano Energy* **83**, 105826 (2021). <https://doi.org/10.1016/j.nanoen.2021.105826>
31. M.A. Migliorato, J. Pal, R. Garg, G. Tse, H.Y.S. Al-Zahrani et al., A review of non linear piezoelectricity in semiconductors. *AIP Conf. Proc.* **1590**, 32 (2014). <https://doi.org/10.1063/1.4870192>
32. R. Hinchet, S. Lee, G. Ardila, L. Montès, M. Mouis et al., Performance optimization of vertical nanowire-based piezoelectric nanogenerators. *Adv. Funct. Mater.* **24**(7), 971–977 (2014). <https://doi.org/10.1002/adfm.201302157>
33. W. Li, Q. Liu, Z. Fang, L. Wang, S. Chen et al., All-solid-state on-chip supercapacitors based on free-standing 4H-SiC nanowire arrays. *Adv. Energy Mater.* **9**(17), 1900073 (2019). <https://doi.org/10.1002/aenm.201900073>
34. C. Chen, S. Chen, M. Shang, F. Gao, Z. Yang et al., Fabrication of highly oriented 4H-SiC gourd-shaped nanowire arrays and their field emission properties. *J. Mater. Chem. C* **4**(23), 5195–5201 (2016). <https://doi.org/10.1039/c6tc00450d>
35. L. Ye, L. Chen, J. Yu, S. Tu, B. Yan et al., High-performance piezoelectric nanogenerator based on electrospun ZnO nanorods/P(VDF-TrFE) composite membranes for energy harvesting application. *J. Mater. Sci. Mater. Electron.* **32**, 3966–3978 (2021). <https://doi.org/10.1007/s10854-020-05138-0>
36. G. Gautier, F. Cayrel, M. Capelle, J. Billoué, X. Song et al., Room light anodic etching of highly doped n-type 4H-SiC in high-concentration HF electrolytes: difference between C and Si crystalline faces. *Nanoscale Res. Lett.* **7**, 367 (2012). <https://doi.org/10.1186/1556-276X-7-367>
37. J.H. Lee, W.J. Lee, S.H. Lee, S.M. Kim, S. Kim et al., Atomic-scale origin of piezoelectricity in wurtzite ZnO. *Phys. Chem. Chem. Phys.* **17**(12), 7857–7863 (2015). <https://doi.org/10.1039/c4cp06094f>
38. A. Onodera, M. Takesada, Electronic ferroelectricity in II-VI semiconductor ZnO. *Advances in Ferroelectrics*, 231–255 (INTECH, 2012) <https://doi.org/10.5772/52304>
39. S. Goel, B. Kumar, A review on piezo-/ferro-electric properties of morphologically diverse ZnO nanostructures. *J. Alloys Compd.* **816**, 152491 (2020). <https://doi.org/10.1016/j.jallcom.2019.152491>
40. S.Q. Liu, K.Z. Huang, W.X. Liu, Z.D. Meng, L. Luo, Cobalt-doped MoS₂ enhances the evolution of hydrogen by piezoelectric catalysis under the 850 nm near-infrared light irradiation. *New J. Chem.* **44**(33), 14291–14298 (2020). <https://doi.org/10.1039/d0nj01053g>
41. Y.K. Dou, J.B. Li, X.Y. Fang, H.B. Jin, M.S. Cao, The enhanced polarization relaxation and excellent high-temperature dielectric properties of N-doped SiC. *Appl. Phys. Lett.* **104**(5), 052102 (2014). <https://doi.org/10.1063/1.4864062>
42. D. Mallick, P. Constantinou, P. Podder, S. Roy, Multi-frequency MEMS electromagnetic energy harvesting. *Sens. Actuat. A Phys.* **264**, 247–259 (2017). <https://doi.org/10.1016/j.sna.2017.08.002>



43. J. Kim, J.H. Lee, H. Ryu, J.H. Lee, U. Khan et al., High-performance piezoelectric, pyroelectric, and triboelectric nanogenerators based on P(VDF-TrFE) with controlled crystallinity and dipole alignment. *Adv. Funct. Mater.* **27**(22), 1700702 (2017). <https://doi.org/10.1002/adfm.201700702>
44. S. Yu, Y. Zhang, Z. Yu, J. Zheng, Y. Wang et al., PANI/PVDF-TrFE porous aerogel bulk piezoelectric and triboelectric hybrid nanogenerator based on in-situ doping and liquid nitrogen quenching. *Nano Energy* **80**, 105519 (2021). <https://doi.org/10.1016/j.nanoen.2020.105519>
45. J. Nie, L. Zhu, W. Zhai, A. Berbille, L. Li et al., Flexible piezoelectric nanogenerators based on P(VDF-TrFE)/CsPbBr₃ quantum dot composite films. *ACS Appl. Electron. Mater.* **3**(5), 2136–2144 (2021). <https://doi.org/10.1021/acsaelm.1c00137>
46. X. Ren, H. Fan, Y. Zhao, Z. Liu, Flexible lead-free BiFeO₃/PDMS-based nanogenerator as piezoelectric energy harvester. *ACS Appl. Mater. Interfaces* **8**(39), 26190–26197 (2016). <https://doi.org/10.1021/acsami.6b04497>
47. S. Liu, D. Zou, X. Yu, Z. Wang, Z. Yang, Transfer-free PZT thin films for flexible nanogenerators derived from a single-step modified sol-gel process on 2D mica. *ACS Appl. Mater. Interfaces* **12**(49), 54991–54999 (2020). <https://doi.org/10.1021/acsami.0c16973>
48. H. Liu, X. Lin, S. Zhang, Y. Huan, S. Huang et al., Enhanced performance of piezoelectric composite nanogenerator based on gradient porous PZT ceramic structure for energy harvesting. *J. Mater. Chem. A* **8**(37), 19631–19640 (2020). <https://doi.org/10.1039/d0ta03054f>
49. H. Su, X. Wang, C. Li, Z. Wang, Y. Wu et al., Enhanced energy harvesting ability of polydimethylsiloxane-BaTiO₃-based flexible piezoelectric nanogenerator for tactile imitation application. *Nano Energy* **83**, 105809 (2021). <https://doi.org/10.1016/j.nanoen.2021.105809>
50. L.Y. Zhu, J.G. Yang, K. Yuan, H.Y. Chen, T. Wang et al., Enhanced piezoelectric performance of the ZnO/AlN stacked nanofilm nanogenerator grown by atomic layer deposition. *APL Mater.* **6**(12), 121109 (2018). <https://doi.org/10.1063/1.5057889>
51. L. Algieri, M.T. Todaro, F. Guido, V. Mastronardi, D. Desmaële et al., Flexible piezoelectric energy-harvesting exploiting biocompatible AlN thin films grown onto spin-coated polyimide layers. *ACS Appl. Energy Mater.* **1**(10), 5203–5210 (2018). <https://doi.org/10.1021/acsaem.8b00820>